Ahmed M. Alwan
Ahmad A. Nimah

Department of Physics,
College of Science,
University of Baghdad,
Baghdad, IRAQ

Effects of Laser Energy on Characteristics of Plasma Produced by Laser Ablation of Ni-Ti Targets

This work shows aims to study the effect of plasma characteristics induced by a pulsed laser from a nickel-titanium (Ni-Ti) target at varying laser energy with the composition phase, structural, and surface morphology of the ablated nanoparticles. The increasing intensity of Ti II lines at higher energies, while absent of nickel, indicates differences between the excitation capabilities of the two metals. The electron temperature increases with the pulse energy, affecting the crystallinity and phase composition of the prepared nanoparticles. The plasma density increased with the laser energy due to the rise in the ionisation process. The XRD analysis of Ni/Ti NPs demonstrates that increasing laser energy leads to an increase in the Ni phase, enhanced crystallinity, and reduced strain in the nanoparticles. The FE-SEM images confirm the variation in morphology with increasing laser energy, enhancing the particles' uniformity. The 900 mJ laser energy ablation is more suitable for applications requiring high density such as in biomedical implants.

Keywords: Plasma characteristics; Ni/Ti NPs; Structural properties; Laser ablation
Received: 4 April 2025; **Revised:** 12 May 2025; **Accepted:** 19 May 2025

1. Introduction

Nitinol (NiTi), a nickel-titanium alloy, receives significant attention for different fields of applications due to its exceptional properties, including shape memory and superelasticity [1]. NiTi nanoparticles have low toxicity and noble biocompatibility, which makes them candidates for implant coatings [2]. NiTi nanoparticles can also be used to coat biomedical devices such as surgical instruments [3]. NiTi NP was found to be angiogenic, which extends its applicability in tissue engineering [4]. NiTi NPs strongly depend on the proportion of the two elements and the grain size [5].

Pulsed laser ablation in liquid (PLAL) has developed as an active route for synthesizing nanomaterials. It is an environmentally friendly and cost-effective approach with controlled structural and morphological properties of the prepared nanoparticles [6,7]. The PLAL technique produce high-purity nanoparticles (NPs) without additional agents, making it advantageous for biomedical applications [8]. The formation of nanoparticles by PLAL is governed by complex physical and chemical processes within the laser-induced plasma [9], affected by laser parameters such as pulse energy, wavelength, and pulse duration [10,11].

The plasma characteristics, including electron temperature (T_e) and their number density (n_e), are essential factors that affect the characteristics of the ablated nanoparticles [12]. The energy distribution within the plasma directly affects the vaporization of target material, nucleation and particle growth [13].

Optical emission spectroscopy (OES) is a powerful technique for plasma diagnosis by examining the emission spectra of excited species within the plasma [14]. This technique gives provides date about plasma conditions, which correlate with the structural and chemical properties of the synthesized nanoparticles [15]. It can also be used to control nanoparticle composition, enhancing their suitability for biomedical applications [16].

This study aims to investigate the effect of laser energy on the plasma characteristics induced near the surface of the Ni/Ti target and their correlation with the structural and morphological properties of the created alloy nanoparticles. The research focuses on the phase change of the generated phases with the laser energy.

2. Experimental Part

The OES was used to investigate the plasma characteristics during pulsed laser ablation of Ni/Ti nanoparticles (NPs) at different laser energies. The correlation between laser energy with both plasma characteristics and the properties of the generated nanoparticles was examined. A target was prepared by my mixing nickel and titanium powders at a 50/50 Ni/Ti atomic ratio using a ball mill, followed by pressing under 5 tons of pressure to form a 2.0 cm diameter disk. An Nd:YAG laser (Diamond-288) with a wavelength of 1064 nm was employed at varying pulse energies (600, 700, 800, and 900 mJ) Plasma characteristics were analyzed using a spectrometer (Thorlabs-CCS 100/M) over a wavelength range of 200 to 400 nm. For each sample, 200 laser pulses were applied. The synthesized Ni/Ti nanoparticles were than drop-cast onto a glass substrate and dried at 70°C for further characterization.

The structural properties and phase composition of the deposited nanoparticles (prepared at different laser energies) were analyzed using SHIMADZU-6000 X-ray diffractometer. The morphology of the samples

was introduced by an Inspect F50, FEI field-emission scanning electron microscopy (FE-SEM).

3. Results and Discussion

Figure (1) displays the plasma emission spectral generated during laser ablation of a Ni/Ti target across 250 - 700 nm wavelength range ,recorded at four distinct pulse laser energies (600, 700, 800, and 900 mJ). The spectra exhibit characteristic emission lines of titanium (Ti) and nickel (Ni), whose relative intensities show significant energy dependence .All observed spectral features were identified by comparison with reference atomic emission data from the National Institute of Standards and Technology (NIST) [17], confirming the presence of neutral (Ti I, Ni I) and singly-ionized (Ti II, Ni II) in the plasma. The emission intensity increases significantly with rising the laser energy from 600 to 900 mJ. This behaviour results from enhanced ablation rates and greater plasma excitation at higher energy levels generating more excited atoms and molecular species [18,19].

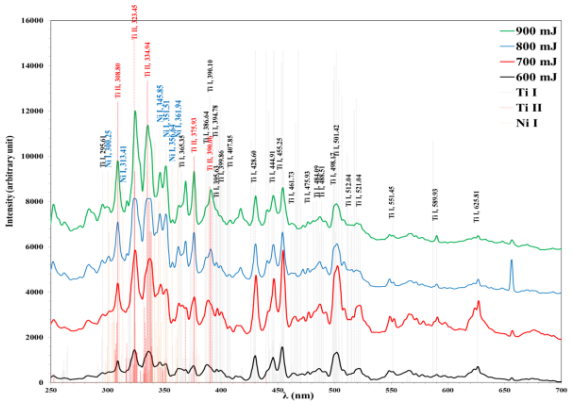

Fig. (1) Plasma emission spectra of the laser induced plasma at different pulse energies from Ni/Ti target

The appearance of neutral titanium spectral lines (Ti I) indicates a substantial portion of the ablated species remains in the ground state. The intensification of single-ionized titanium lines (Ti II) with increasing laser energy confirms elevated plasma temperatures. In contract, nickel demonstrates significantly higher resistance to ionization under these experimental conditions.

Variation in emission lines intensities accurately reflect relative changes in the plasma species concentrations, though they cannot determine absolute quantities due to the determine of the spectral intensity on multiple factors including transition probability, statistical weight of energy levels , and instrument characteristics .Consequently ,this technique reveals trends in particle distribution dynamics rather than providing absolute concentration measurements.

Figure (2) presents the emission intensity variation of selected spectral line corresponding to the Ni I (351.51 nm) and Ti I (455.25 nm), along with their intensity ratio as a function of laser energy .Analysis reveals significantly stronger laser energy dependence for Ni emission compared to Ti, with Ni I line intensity being substantially weaker than Ti I lower laser energy. This observed display primarily originates from fundamental differences in the materials physical and thermodynamic properties, particularly their binding energy, thermal conductivities, and vaporization temperature [20]. Titanium‘s characteristically lower density and reduced thermal conductivity than Ni, contributing to a higher initial ablation rate of Ti at lower laser energies to overcome its binding forces and vaporization initiate than Ni [21].

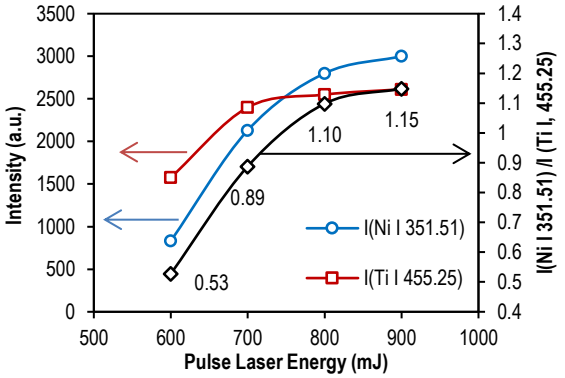

Fig. (2) Variation of emission line intensity of the Ni I (351.51 nm) and Ti I (455.25 nm) and their ratio

The intensity of both Ni and Ti emission lines increases with the laser energy. However, the rate of growth is more distinct for Ni compared with Ti. The increase in intensity indicates enhance ablation efficiency of Ni and increasing the excitation probability of Ni species in the plasma. The ratio of Ni I (351.51 nm) to Ti I (455.25 nm) emission intensities increased with increasing laser energy. The observed trends indicate the significance of laser energy in controlling the relative ablation of Ni and Ti, which are governed by their intrinsic material properties and interaction dynamics with the laser pulse [22].

As shown in Fig. (3), the Boltzmann plot analysis used to determines the induced plasma's electron temperature (T_e) of the induced plasma during Ni/Ti thin film deposition. Based on the fundamental assumption that plasma excitation follows a Boltzmann distribution. T_e is derived from the inverse slope of the linear fit in the Boltzmann plot, utility NIST atomic data for Ti I emission listed in table (1). The observed linear relationship strongly validates of the experimental data. T_e increases with the increase in laser energy. This temperature is elevation results directly from greater energy deposition into the plasma at higher laser energies, which promotes more efficient excitation of atomic species to elevated electronic states.

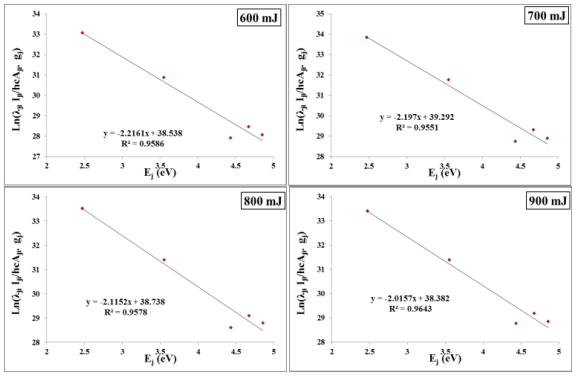

Fig. (3) Boltzmann-plot at different laser energies using the Ti I emission lines

Table (1) The NIST data corresponding to the used Ti I emission lines in Boltzmann plot

Wavelength (nm)	$g_kA_{ki}\times10^8$	E_i (eV)	E_j (eV)
444.9143	11.0	1.887	4.67301
453.3240	9.71	0.848	3.58265
461.7268	7.66	1.749	4.43335
475.8118	7.84	2.249	4.85424
499.1067	6.42	0.836	3.31943

The elevated electron temperature significantly the ablation dynamics by enhancing the kinetic energy of the ablated species, which improving atomic mobility during film formation [23]. This effect manifests in the resulting thin films through two key structural improvements: increased crystallite sizes and reduced internal strain. Also, the substantially higher plasma temperature at 900 mJ creates a strongly ionized environment, which may contribute to oxidation processes when oxygen is present in the deposition chamber.

Figure (4) shows the Lorentzian fitting analysis of the Ti II 308.80 nm emission line, which illustrates the influence of laser energy on the spectral broadening in the laser-induced Ni-Ti plasma. The observed broadening primarily results from Stark effects, while minor broadening mechanisms related to electron number density (n_e) are neglected. Stark broadening originates from the electric field generated by free electrons surrounding emitting species. The full width at half maximum ($\Delta\lambda$) exhibits a progressive increases from 600 to 900 mJ, directly high laser energies. This relationship stems from increased ionization efficiency at elevated energies, yielding higher free electrons concentration.

Plasma density (n_e) is quantitatively determined through Stark broadening according to the relation $n_e = (\frac{\Delta\lambda}{2\omega_s})\ N_r$ [15], where ω_s is the electron impact parameter for Ti II at 308.80 nm, Nr is the reference electron density [24], and $\Delta\lambda$ is the determined line's broadening

Table (2) displays the plasma parameters induced by laser ablation of a Ni/Ti target at the different pulse energies. The electron temperature increases from 0.451 to 0.496 eV while the electron density from 3.913×10^{17} to 5.507×10^{17} cm^{-3} as the laser pulse energy increases from 600 to 900 mJ. The higher electron temperature causes more ionization, resulting in more free electrons in the plasma plume.

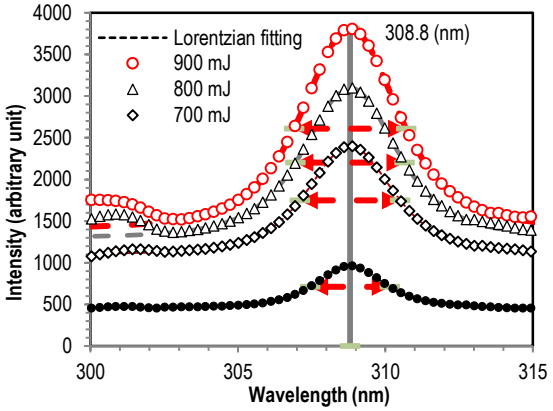

Fig. (4) Lorentzian fit for Ti II, 308.80 nm line at different pulse energies

Table (2) Plasma parameters at different pulse energies from the Ni/Ti target

E (mJ)	T_e (eV)	$n_e\times10^{17}$ (cm^{-3})	f_p (Hz) $\times10^{10}$	$\lambda_D\times10^{-5}$(cm)	N_D
600	0.451	3.913	561.738	0.798	833
700	0.455	4.928	630.364	0.714	752
800	0.473	5.362	657.586	0.698	763
900	0.496	5.507	666.413	0.705	809

The plasma frequency, which describes the oscillation of free electrons in response to external fields, also exhibits a rising trend corresponding to the rise in electron density. The Debye length shows a decreasing trend as laser energy increases due to a stronger Coulomb interaction within the plasma due to increased electron density. These results influence plasma behaviour and its interactions with surrounding materials. The number of particles within a Debye sphere (N_D) exhibits fluctuations across different pulse energies.

Figure (5) displays the XRD patterns of the deposited Ni/Ti NPs prepared by PLA at 600, 700, 800, and 900 mJ pulse laser energies. The diffraction peaks observed correspond to different crystalline phases of the hexagonal Ti phase and cubic Ni phase, and there is a minor presence of cubic NiO, according to the JCPDS card no. 96-900-8518, 03-1051, and 96-432-0488, respectively.

The crystallite size, determined using the Scherrer formula [25] $D = \frac{0.9\,\lambda}{\beta.cos(\theta)}$ where β is the breadth of a diffraction line, and θ is the diffraction angle. The D values increase with increasing laser energy. The crystallite size of Ni increases from 16.5 nm at 600 mJ to 19.3 nm at 900 mJ, indicating grain growth at higher laser fluences. Similarly, the crystallite size of

Ti increases slightly, although at a slower rate compared to Ni.

The lattice strain ($\boldsymbol{\varepsilon}$) was calculated according to the relation [26] $\varepsilon = \frac{\beta.cot(\theta)}{4}$. The ε values decreas as the laser energy increases. The higher strain at low laser energy due to rapid condensation of ablated species and limited atomic rearrangement. As the laser energy increases, the additional energy allows strain relaxation, resulting in improved crystallinity. The increasing Ni content and reduced strain at higher laser energy may alter the mechanical and functional characteristics of the thin films, making them more suitable for applications such as biomedical coatings. Table (3) displays the XRD parameters of Ni/Ti thin films deposited by different laser pulse energies.

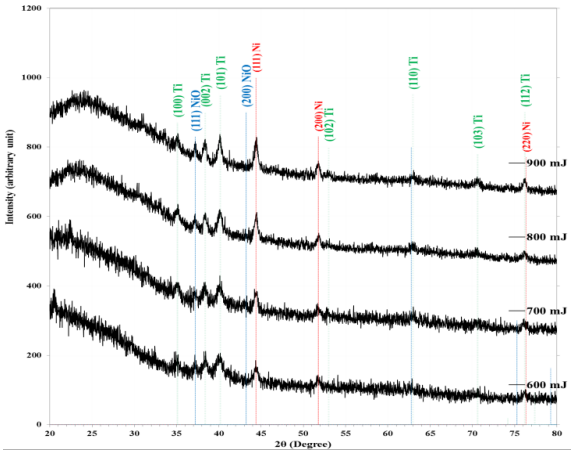

Fig. (5) XRD of the as-deposited Ni/Ti composite films using different pulse laser energies

As the laser energy increases, an evident variation in the phase composition is observed. The phase ratios for Ti and Ni were determined according to the summation of intensities corresponding to diffraction lines, as listed in table (4). At 600 mJ, the film mainly comprises the Ti phase, making up 60.8% of the total composition, while the Ni phase accounts for only 31.7%. The dominance of Ti at lower laser energy suggests that the ablation rate of Ti is initially higher due to differences in material properties. However, as the laser energy increases, the Ni phase percentage increases progressively, reaching 38.0% at 900 mJ due to the enhanced ablation efficiency of Ni. Since Ni has a higher density and thermal conductivity than Ti, it requires more significant energy input to reach the vaporization threshold.

Figure (6) displays the top-view FE-SEM micrographs at two magnifications (30 kx and 120 kx) examining morphological variations in Ni/Ti NPs synthesized at 600 mJ and 900 mJ laser energies. The 600 mJ samples demonstrate characterized by larger nanoparticles (64-99 nm diameter range) with irregular packed and pronounced clustering, this morphological behavior stems from reduced likely kinetic energy of the ablated species at lower laser energies, resulting inefficient surface diffusion and non-uniform particle dispersion during deposition. In contrast, the 900 mJ samples exhibit significantly improved morphological characteristics, featuring smaller nanoparticles (20-55 nm diameter range) with enhances size uniformity and spatial distribution. This transformation arises from increased laser fluence, which promotes more efficient energy transfer to the target material, thereby improving sputtering yield and nanoparticles refinement. The higher deposition energy simultaneously induces two beneficial effects: greater film densification and reduced surface roughness. The improved uniformity at 900 mJ can be attributed to higher plasma density.

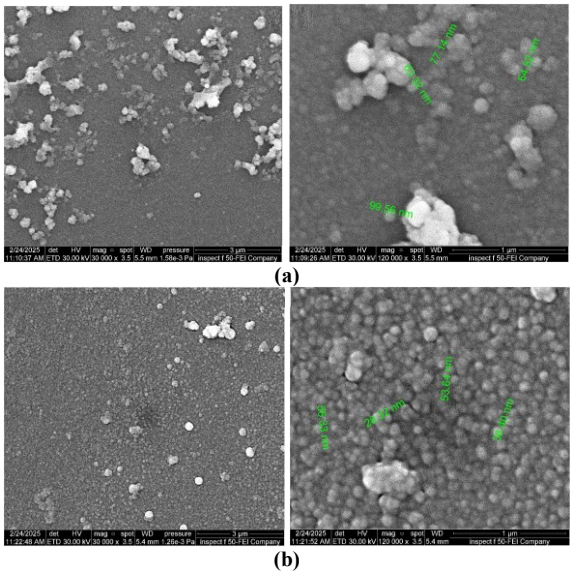

Fig. (6) FE-SEM images of as-deposited Ni/Ti films on glass slides at (a) 600 mJ and (b) 900 mJ laser energies

Table (4) Phase composition percentages according to the XRD peak intensities

Phase	600 mJ	700 mJ	800 mJ	900 mJ
Ni	31.7%	32.9%	35.5%	38.0%
Ti	60.8%	59.3%	56.2%	53.0%
NiO	7.5%	7.8%	8.4%	9.0%

4. Conclusion

A strong relationship between laser energy and ionization degree was revealed. The increasing intensity of Ti II lines at higher laser energies indicates an increasing ionization, whereas Ni I lines dominate with minimal ionization. The critical role of laser energy in modifying plasma properties for thin-film deposition was confirmed. Increasing laser energy leads to elevate electron temperature, higher plasma density, and increase ablated material at rates dependent on material characteristics, significantly affecting the physical and chemical properties of the deposited Ni-Ti NPs. The higher laser energy results in increased Ni content, larger crystallite size, and

reduced strain, all contributing to variation in the thin film properties. Moreover, increasing laser energy improves film uniformity. Films deposited at 900 mJ exhibits superior density, making it highly suitable for applications requiring high-quality coatings, such as biomedical implants.

References

[1] S.K. Patel et al., "A review on NiTi alloys for biomedical applications and their biocompatibility", *Mater. Today Proc.*, 33 (2020) 5548–5551.

[2] X. Li et al., "Research progress on surface modification and coating technologies of biomedical NiTi alloys", *Colloids Surf. B Biointerf.*, 249 (2025) 114496.

[3] S. McGlumphy et al., "Biocompatible antibiotic-coupled nickel-titanium nanoparticles as a potential coating material for biomedical devices", *Heliyon*, 10 (2024) e31434.

[4] A.K. Srivastava et al., "Examining the role of nickel and NiTi nanoparticles promoting inflammation and angiogenesis", *J. Immunotoxicol.*, 19 (2022) 61–73.

[5] M. Chakif et al., "Generation of NiTi Nanoparticles by Femtosecond Laser Ablation in Liquid", *J. Mater. Eng. Perform.*, 23 (2014) 2482–2486.

[6] H.J. Imran, K.A. Hubeatir and K.A. Aadim, "A novel method for ZnO@NiO core–shell nanoparticle synthesis using pulse laser ablation in liquid and plasma jet techniques", *Sci. Rep.*, 13 (2023) 5441.

[7] A. Torrisi et al., "Biocompatible nanoparticles production by pulsed laser ablation in liquids", *J. Instrum.*, 15 (2020) C03053–C03053.

[8] N. Baig, I. Kammakakam and W. Falath, "Nanomaterials: a review of synthesis methods, properties, recent progress, and challenges", *Mater. Adv.*, 2 (2021) 1821–1871.

[9] A. Ojeda-G-P, M. Döbeli and T. Lippert, "Influence of Plume Properties on Thin Film Composition in Pulsed Laser Deposition", *Adv. Mater. Interfaces*, 5 (2018) 1–16.

[10] G.M. Al-Senani et al., "Effect of laser pulse repetition rate in the synthesis of nickel oxide nanoparticles in PVA solution on the adsorption efficiency against phosphate ions", *Radiat. Phys. Chem.*, 208 (2023) 110872.

[11] K.A. Aadim, A.A. Hussain and M.R. Abdulameer, "Effect of annealing temperature and laser pulse energy on the optical properties of CuO films prepared by pulsed laser deposition", *Iraqi J. Phys.*, 12 (2014) 97–104.

[12] A. De Giacomo, "Experimental characterization of metallic titanium-laser induced plasma by time and space resolved optical emission spectroscopy", *Spectrochim. Acta B: Atom. Spectro.*, 58 (2003) 71–83.

[13] M.H. Mohsin, K.S. Khashan and G.M. Sulaiman, "Effect of laser parameters on the structural properties of gadolinium oxide nanoparticles synthesis via pulsed laser ablation in liquid", *Eur. Phys. J. B*, 97 (2024) 147.

[14] R.S. Mohammed, K.A. Aadim and K.A. Ahmed, "Synthesis of CuO/ZnO and MgO/ZnO Core/Shell Nanoparticles with Plasma Jets and Study of their Structural and Optical Properties", *Karbala Int. J. Mod. Sci.*, 8 (2022) 88–97.

[15] A. Ajith et al., "Comprehensive Analysis of Copper Plasma: A Laser-Induced Breakdown Spectroscopic Approach", *Photonics*, 10 (2023).

[16] A. Sergievskaya et al., "Magnetron sputter deposition of silver onto castor oil: The effect of plasma parameters on nanoparticle properties", *Colloids Surf. A Physicochem. Eng. Asp.*, 615 (2021) 126286.

[17] NIST Atomic Spectra Database, Online Available at http://Kinetics.Nist.Gov/Index.Php, (2025).

[18] K.A. Aadim and R.H. Jassim, "Determination of plasma parameters and nanomaterial's synthesis of Zn and Mn using laser induced plasma spectroscopy", *AIP Conf. Proc.*, 2372 (2021) 080014.

[19] H. Bolouki and Y. Li, "Emission Spectroscopic Characterization of a Helium Atmospheric Pressure Plasma Jet with Various Mixtures of Argon Gas in the Presence and the Absence of De-Ionized Water as a Target", *Plasma*, 2 (2019) 283–293.

[20] L.M. Doeswijk, G. Rijnders and D.H.A. Blank, "Pulsed laser deposition: Metal versus oxide ablation", *Appl. Phys. A Mater. Sci. Process.*, 78 (2004) 263–268.

[21] P.G. Klemens and R.K. Williams, "Thermal conductivity of metals and alloys", *Int. Met. Rev.*, 31 (1986) 197–215.

[22] S.A. Irimiciuc et al., "Target properties – Plasma dynamics relationship in laser ablation of metals: Common trends for fs, ps and ns irradiation regimes", *Appl. Surf. Sci.*, 506 (2020).

[23] A.S. Maktoof and G.H. Mohammed, "The Effect of Au Nanoparticles on the Structural and Optical Properties of ($NiO:WO_3$) Thin Films Prepared by PLD Technique", *Iraqi J. Sci.*, 63 (2022) 2502–2513.

[24] D. Tankosić, L.Č. Popović and M.S. Dimitrijević, "Electron-Impact Stark Broadening Parameters for Ti II And Ti III Spectral Lines", *Atom. Data Nucl. Data Tables*, 77 (2001) 277–310.

[25] H.E. Swanson, H.F. McMurdie, M.C. Morris, E.H. Evans, and B. Paretzkin, **"Standard X-ray**

Diffraction Powder Patterns", National Bureau of Standards (NBS), monograph 25, section 9 (1971).

[26] A.A. Meji, D. Usha and B.M. Ashwin, "Microwave-assisted green synthesis of zinc oxide nanoparticles using pistia stratiotes for anticancer and antibacterial applications", *Mater. Res. Exp.*, 11 (2024) 085004.

Table (3) XRD parameters of Ni/Ti thin films at different laser energies

Laser Energy (mJ)	2θ (°)	FWHM (°)	d_{hkl} (Å)	D (nm)	Phase	hkl	Strain
600	35.0660	0.5855	2.5570	14.2	Hex. Ti	(100)	0.0081
	37.1770	0.4479	2.4165	18.7	Cub. NiO	(111)	0.0058
	38.3500	0.5855	2.3452	14.4	Hex. Ti	(002)	0.0073
	40.0880	0.7143	2.2475	11.8	Hex. Ti	(101)	0.0085
	44.3860	0.5215	2.0393	16.5	Cub. Ni	(111)	0.0056
	51.7390	0.5326	1.7654	16.6	Cub. Ni	(200)	0.0048
700	35.0780	0.5555	2.5561	15.0	Hex. Ti	(100)	0.0077
	37.1890	0.4249	2.4157	19.7	Cub. NiO	(111)	0.0055
	38.3620	0.5555	2.3445	15.1	Hex. Ti	(002)	0.0070
	40.1000	0.6777	2.2468	12.5	Hex. Ti	(101)	0.0081
	44.3980	0.4948	2.0388	17.3	Cub. Ni	(111)	0.0053
	51.7510	0.5054	1.7651	17.5	Cub. Ni	(200)	0.0045
800	35.0900	0.5270	2.5553	15.8	Hex. Ti	(100)	0.0073
	37.2010	0.4032	2.4150	20.8	Cub. NiO	(111)	0.0052
	38.3740	0.5270	2.3438	16.0	Hex. Ti	(002)	0.0066
	40.1120	0.6429	2.2462	13.2	Hex. Ti	(101)	0.0077
	44.4100	0.4695	2.0383	18.3	Cub. Ni	(111)	0.0050
	51.7630	0.4795	1.7647	18.4	Cub. Ni	(200)	0.0043
900	35.1020	0.5000	2.5544	16.7	Hex. Ti	(100)	0.0069
	37.2130	0.3825	2.4142	21.9	Cub. NiO	(111)	0.0050
	38.3860	0.5000	2.3431	16.8	Hex. Ti	(002)	0.0063
	40.1240	0.6100	2.2455	13.9	Hex. Ti	(101)	0.0073
	44.4220	0.4454	2.0377	19.3	Cub. Ni	(111)	0.0048
	51.7750	0.4549	1.7643	19.4	Cub. Ni	(200)	0.0041

